Vesicles in electric fields: Some novel aspects of membrane behavior†

Rumiana Dimova,[*a] **Natalya Bezlyepkina,**[a] **Marie Domange Jordö,**[b] **Roland L. Knorr,**[a] **Karin A. Riske,**[c] **Margarita Staykova,**[a] **Petia M. Vlahovska,**[d] **Tetsuya Yamamoto,**[a] **Peng Yang‡**[a] **and Reinhard Lipowsky**[a]

This review focuses on the effects of electric fields on giant unilamellar vesicles, a cell-size membrane system. We describe various types of behavior of vesicles subjected to either alternating fields or strong direct current pulses, such as electrodeformation, -poration and -fusion. The vesicle response to alternating fields in various medium conditions is introduced and the underlying physical mechanisms are highlighted, supported by theoretical modeling. New aspects of the response of vesicles with charged or neutral membranes, in fluid or gel-phase, and embedded in different solutions, to strong direct current pulses are described including novel applications of vesicle electrofusion for nanoparticle synthesis.

1.   Introduction

The response of biological membranes and cells to electric fields has received a lot of attention, both because of fundamental interest and because of potential practical applications. External electric fields, whether weak alternating (AC) fields or strong direct current (DC) pulses, have emerged as a powerful method for cell manipulation in biomedical and biotechnological applications. For example, electric fields are employed in novel *in-vivo* and *in-situ* applications for tissue ablation, wound healing and cancer treatment.[1–6] Strong electric fields can cause a significant increase in the electric conductivity and permeability of the cell plasma membrane. This phenomenon, also referred to as electroporation or electropermeabilization, is used for introducing various molecules into the cell, to which the membrane is otherwise impermeable.[7,8] Because of its efficiency, this method is rapidly becoming an established approach for treatment of carcinoma, melanoma and connective tissue cancer,[9–12] and it also holds great promise for gene therapy.[13,14] Membrane electroporation and electrofusion are of particular interest because these methods are widely used in cell biology and biotechnology as means for cell hybridization.[15]

Synthetic lipid vesicles provide biomembrane models suitable for systematic investigations of the impact of electric fields on lipid bilayers. Studies on small vesicles with a size about 100 nm[16–18] and on giant unilamellar vesicles with a diameter of several tens of microns,[19–31] have been performed to elucidate the response of the membrane to electric fields; for a partial overview see Dimova *et al.*[32] Membrane behavior in electric fields is a topic of active research. Here, we will focus mainly on new developments by our group. Even though we will attempt to cite all important contributions in the field, the selection is subjective and far from being exhaustive.

The paper is organized as follows; first we introduce some basic timescales that govern the interaction of electric fields with membranes. Then we consider the response of vesicles to AC fields and DC pulses, discussing some new observations (both reported and not yet published). We conclude with a short outlook.

2.   Membranes in electric fields: some relations

The response of membranes to electric fields involves dynamic physical processes occurring on different time scales. Free charges accumulate on boundaries separating media with different electric properties. A spherical vesicle polarizes on the Maxwell–Wagner time scale[33]

$$t_{\mathrm{MW}} = \frac{\varepsilon_{\mathrm{in}} + 2\varepsilon_{\mathrm{ex}}}{\lambda_{\mathrm{in}} + 2\lambda_{\mathrm{ex}}} \qquad (1)$$

where $\varepsilon_{\mathrm{in}}$ and $\varepsilon_{\mathrm{ex}}$ are the dielectric constants, and λ_{in} and λ_{ex} are the conductivities of the solutions inside and outside the vesicle, respectively.

The lipid bilayer is impermeable to ions and free charges pile up on both membrane surfaces. Hence, the vesicle acts as a capacitor, which charges on a time scale[34,35]

$$t_{\mathrm{c}} = RC_{\mathrm{m}} \left(\frac{1}{\lambda_{\mathrm{in}}} + \frac{1}{2\lambda_{\mathrm{ex}}} \right) \qquad (2)$$

where R is the vesicle radius and C_{m} is the membrane capacitance.

The capacitor charging time t_{c} is typically much longer than the Maxwell–Wagner time t_{MW}. For example, we can estimate $t_{\mathrm{c}} \sim 10$ μs and $t_{\mathrm{MW}} \sim 0.01$ μs for conditions corresponding to experiments on vesicles in 1 mM NaCl, namely $\varepsilon_{\mathrm{in}} \sim \varepsilon_{\mathrm{ex}} = 80\varepsilon_0$,

[a]*Max Planck Institute of Colloids and Interfaces, Science Park Golm, 14424 Potsdam, Germany. E-mail: Rumiana.Dimova@mpikg.mpg.de; Fax: +49 331 567 9615; Tel: +49 331 567 9612*
[b]*Niels Bohr Institute, University of Copenhagen, Blegdamsvej 17, 2100 Copenhagen, Denmark*
[c]*Depto. de Biofísica, Universidade Federal de São Paulo, R. Botucatu, 862, CEP 04023-062 São Paulo, Brazil*
[d]*Thayer School of Engineering, Dartmouth College, Hanover, NH, 03755, USA*

where ε_0 is the vacuum permittivity, $\lambda_{in} \sim \lambda_{ex} \sim 10$ mS/m, $C_m \sim 0.01$ F/m², and $R \sim 10$ μm.

These time scales are a key to understanding the dynamic response of vesicles subjected to short electric pulses discussed in section 4, as well as frequency dependence of vesicle deformation discussed in section 3. Note that characteristic angular frequencies are defined as the inverse of the time scales in eqn (1) and (2), e.g. $\omega_{MW} = 1/t_{MW}$. The experimental frequency, ν, is related to the angular one via $\nu = \omega/2\pi$.

3. Vesicle response to AC fields

When subject to AC fields, cells and vesicles can deform. Studies of cell deformation in AC fields have been carried out by many groups and effects on the cell shape, motility and orientation have been reported.[26,36–38] Vesicle deformations have been treated both experimentally and theoretically, but a comprehensive description reconciling observations and calculations is still to emerge.

A detailed understanding of the membrane behavior in AC fields is important for various electromanipulation techniques, as well as for vesicle electroformation protocols[39,40] (including some of the recent developments[41–45]). Even though vesicle electroformation is widely used, the underlying mechanism is not well understood.[46,47] This motivates further studies on effects of AC fields on membranes. Most of the current research in this direction as well as the following sections 3.1 and 3.2 has focused on lipid bilayers with only a few components, whereas biological membranes contain a large number of different components. Bridging the gap would require the exploration of more complex systems.

3.1 Vesicle deformation in AC fields

The deformation of vesicles subjected to AC fields depends on the field frequency ω (or ν) and the conductivity conditions. The latter can be described by the ratio between the internal and the external conductivities λ_{in} and λ_{ex}:

$$x = \lambda_{in}/\lambda_{ex} \qquad (3)$$

Systematically varying the field frequency and solution conductivities allowed us to construct a morphological diagram of the shape transitions observed in phosphatidylcholine vesicles;[48] see Fig. 1a. At high frequencies, the vesicles are spherical independently of x. As the frequency decreases, vesicles with $x > 1$, i.e., with the internal salinity higher than the external one become prolate ellipsoids corresponding to transition 1 in Fig. 1a, while vesicles with $x < 1$ adopt oblate shapes after undergoing transition 2. Further decrease in frequency changes the vesicle shape at transition 4 from oblate to prolate for $x < 1$. For intermediate frequencies an oblate vesicle can become prolate at transition 3.

Theoretical studies of vesicle deformation in AC fields have been limited to rather simple systems. For example, these studies omit the asymmetry in the media conductivities,[24,25,27] and their theoretical predictions are at odds with experiments; see e.g. the supplementary material of Aranda et al.[48] Our recent progress
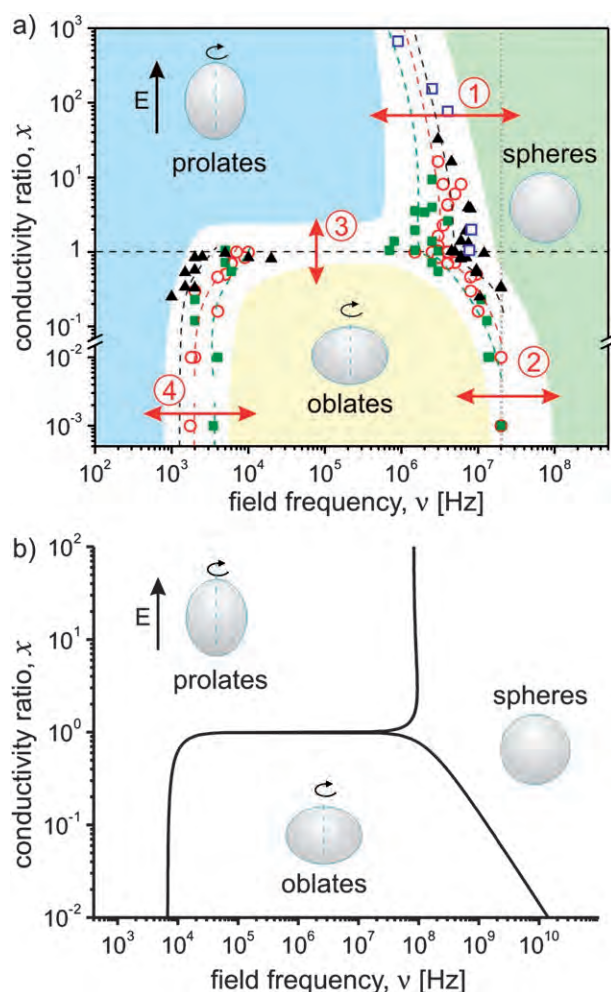

Fig. 1 Morphological diagram of the shapes of vesicles at different conductivity conditions and various field frequencies (a) as determined experimentally, and (b) theoretically predicted for $\lambda_{in} = 6.5$ mS/m. The symbols in (a) correspond to different internal conductivity, λ_{in}, in units mS/m: 1.5 (solid squares), 6.5 (open circles), 13 (solid triangles), 1000 (open squares). The dashed lines are guides to the eye and the shaded areas indicate zones of specific morphology. The four types of morphological transitions are discussed in the text. The dotted vertical line in (a) shows the experimentally accessible frequency limit ($\nu = 2 \times 10^7$ Hz). Schematic views of the vesicle shapes are included as insets and the electric field is indicated by an arrow.

towards realistic theoretical modeling is discussed in the next two sections.

3.1.1 Morphological diagram: energy minimization approach.
Vesicle shapes in AC fields can be investigated within the framework of the energy minimization approach introduced by Winterhalter and Helfrich.[24] The original work, however, is limited to symmetric conductivity conditions with $x = 1$ and thus the model predicts only prolate shapes independent of x. We extended the Winterhalter–Helfrich model to asymmetric conductivity conditions with $x \neq 1$.

The electric field deforms a vesicle from a sphere with radius R into an ellipsoid. The vesicle deformation s_2 is assumed to be small with $s_2 \ll R$; see also Fig. 2a for definition of s_2. Prolate and
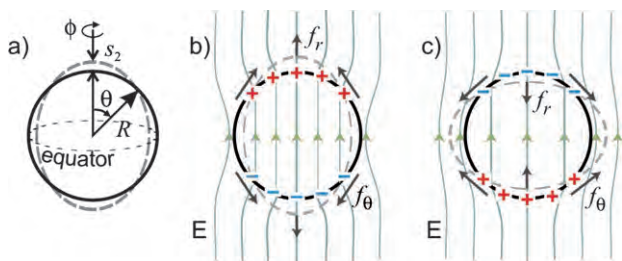
Fig. 2 (a) The vesicle geometry and (b, c) the net charge distribution Q at the vesicle interfaces at intermediate frequencies. Due to the difference in the conductivity conditions, the net charges across the membrane, illustrated with pluses and minuses, differ depending on the value of the conductivity ratio x. The forces (f_r and f_θ) applied to the charges by the normal and the tangential electric fields deform the vesicles into prolates for $x > 1$ (b) and oblates for $x < 1$ (c).

oblate shapes correspond to $s_2 > 0$ and $s_2 < 0$, respectively. The free energy of a vesicle in AC electric fields can be presented as $F = F_{bend} - W$, where F_{bend} is the bending energy of the vesicle in the elliptic deformation, and W is the work done by the Maxwell stresses arising from the electric fields. The deformation s_2 can be determined by minimizing the free energy F or by balancing stresses exerted on the membrane as in section 3.1.2. Fig. 1b shows the morphological diagram predicted by the model just described. The shapes of the boundaries and the transition frequencies agree well with the experimentally determined morphological diagram as shown in Fig. 1a.

The physical mechanism responsible for the vesicle electro-deformation is the interplay between the electric field partitioning in normal and tangential components, and the charging of the membrane interfaces. The lipid bilayer is an insulator, and acts as a capacitor. At low frequencies, $\omega \ll 1/t_c$, the large membrane impedance blocks current from flowing into the vesicle interior and the electric field lines are tangent to the membrane. The vesicle is squeezed at the equator and pulled at the poles by the radial Maxwell stress or pressure arising from the tangential electric field. As a result, the vesicle adopts a prolate shape.

At intermediate frequencies, $1/t_c < \omega < \omega_{MW}$, the membrane is capacitively short-circuited and displacement currents flow through it. The electric field lines penetrate the vesicle interior and the electric field acquires a component normal to the membrane. Because of $x \neq 1$, *i.e.*, of the asymmetry of the internal and external conductivities, the charge densities on the inner and outer membrane interfaces become imbalanced. Within the continuum theory, these charges arise from the discontinuity of the permittivities across the interfaces and represent local accumulation of cations and anions at these interfaces. The resulting net free charge density Q is given by

$$Q(t) = 3E_0\cos\theta \frac{\lambda_{ex}\lambda_{in}}{2\lambda_{ex} + \lambda_{in}}\left(\frac{\varepsilon_{ex}}{\lambda_{ex}} - \frac{\varepsilon_{in}}{\lambda_{in}}\right)\frac{\cos(\omega t + \phi)}{\sqrt{1 + \omega^2/\omega_{MW}{}^2}} \quad (4)$$

where E_0 is the magnitude of the external electric field, and θ and ϕ are the polar and azimuthal angles, respectively; see Fig. 2a. A schematic snapshot of Q is sketched in Fig. 2b and 2c. If $\varepsilon_{ex} \sim \varepsilon_{in}$, the sign of Q is determined solely by the conductivity ratio. The interaction of the tangential and normal electric fields with the free charges produces lateral and normal forces, f_θ and f_r,

respectively. Depending on the polarity of Q, f_θ is directed either towards the poles or the equator, and f_r is directed towards or away from the electrodes, leading to prolate or oblate vesicle shapes as sketched in Fig. 2b, c.[49]

In the high frequency regime, $\omega > \omega_{MW}$, the electric charges cannot follow the oscillations of the electric fields. As a result, the net charge density, Q, as defined in eqn (4), decreases with the field frequency. This relaxes the shape of the vesicle from prolate ($x > 1$) or oblate ($x < 1$) to spherical (transitions 1 and 2 in Fig. 1).

In summary, the charging dynamics of the membrane surfaces and the radial and shear Maxwell stresses play a key role in determining the vesicle morphology in AC fields. The frequency of transition 4 in Fig. 1a corresponds to the inverse charging time of the membrane capacitor, $1/t_c$, and frequency transitions 1 and 2—to the Maxwell–Wagner frequency ω_{MW}.

Quantitatively, the present theory provides reasonable values of the relative vesicle deformation s_2/R (~ 0.1) for small vesicles with size of the linear order of 1 μm. For giant vesicles ($R \sim 10$–100 μm), the theory gives unreasonably large values for s_2/R ($\sim 10^3$–10^6!). However, the shapes of the boundaries in the morphological diagram and the order of the transition frequencies agree with the experiment very well; see Fig. 1. The work W done by the Maxwell stresses is small at the vicinity of the transition frequencies and for small vesicles. Therefore, the present theory shows quantitative agreements with the experiments when W is small. It is necessary to take into account tension and hydrodynamic forces in order to achieve quantitative agreement with the experiments as discussed in the following section.

3.1.2 Vesicle deformation: force balance approach. Another method to determine the vesicle deformation in electric fields is based on the balance of all forces exerted on the membrane[49]

$$\mathbf{n} \bullet \left(\mathbf{T}^{ex} - \mathbf{T}^{in}\right) = \left[2\sigma H - \frac{\delta F_{bend}}{\delta r}\right]\mathbf{n} + \nabla_s\sigma \quad (5)$$

Here $\mathbf{n}$ a is normal vector to the vesicle membrane, $\mathbf{T}^{ex}$ and $\mathbf{T}^{in}$ denote the exterior and interior Maxwell stress, H is the mean curvature, r is the radial coordinate, and σ is the membrane tension.

An essential feature of this approach is the consideration of a variable membrane tension. First, flattening of the shape fluctuations due to vesicle elongation increases the homogeneous part of the tension. Second, because the membrane is nearly incompressible, the tension can become nonuniform along the surface. The resulting gradients in the tension, $\nabla_s\sigma$, are particularly important in the intermediate frequency regime, $1/t_c < \omega < \omega_{MW}$, in which the shear Maxwell stresses are significant and oblate shapes are observed.

For small deviations from sphericity, eqn (5) yields

$$s_2 = R\frac{3p^{el} - 2\tau^{el}}{12(6 + \sigma_h)} \quad (6)$$

where σ_h is the homogeneous tension (which is independent of position along the vesicle surface) and p^{el} and τ^{el} are the maximal values of the difference of the radial and shear Maxwell stresses across the membrane (the expressions for p^{el} and τ^{el} can be found

in Vlahovska *et al.*[49]). For a quasi-spherical vesicle, the homogeneous tension σ_h increases with the apparent area as[50,51]

$$\sigma_h = \sigma_0 \exp\left(\frac{16\pi}{5}\frac{\kappa}{k_B T}s_2^2\right) \qquad (7)$$

where σ_0 is the initial membrane tension, κ is the membrane bending stiffness and $k_B T$ is thermal energy. Eqn (6) is a generalization of the Kummrow–Helfrich result[28] (see eqn (10) in section 3.1.3), which is strictly valid only for low frequencies ($\omega < 1/t_c$), where the shear Maxwell stress is zero. If $x < 1$, the numerator in eqn (6) changes sign at $\omega = 1/t_c$, which marks the prolate–oblate transition (transition 4 in Fig. 1a).

Vesicle shapes computed from eqn (6) are consistent with the experiment, see Fig. 3 (note that the vesicle semiaxis is simply $a = R + s_2$). The discrepancy in the high-frequency oblate–sphere transition frequency for $x < 1$ is presumably due to electric double layer effects.[49] The mechanical approach also explains why the energy approach (section 3.1.1) overestimates the vesicle deformation in strong fields. The reason is that the free energy balance does not take into account the tension. In strong electric fields, the membrane tension controls the extent of vesicle deformation.

3.1.3 Electrodeformation of vesicles as a method to determine the membrane bending stiffness.
Vesicle deformation induced by AC fields can be used to measure the bending stiffness of membranes following the approach developed by Helfrich and coworkers.[28,30] The protocol of such measurements consists of subjecting a vesicle to an AC electric field of increasing strength and recording the induced deformation. One example of vesicle elongation due to stepwise increase in the field strength is shown in Fig. 4a. The degree of deformation is expressed as the aspect ratio a/b, where a and b are the vesicle semiaxes along and perpendicular to the field direction, respectively; see inset in Fig. 4a. Observations of the response time of different vesicles suggest that typically 2 s are sufficient to reach the equilibrium deformation after changing the field strength. Images recorded in
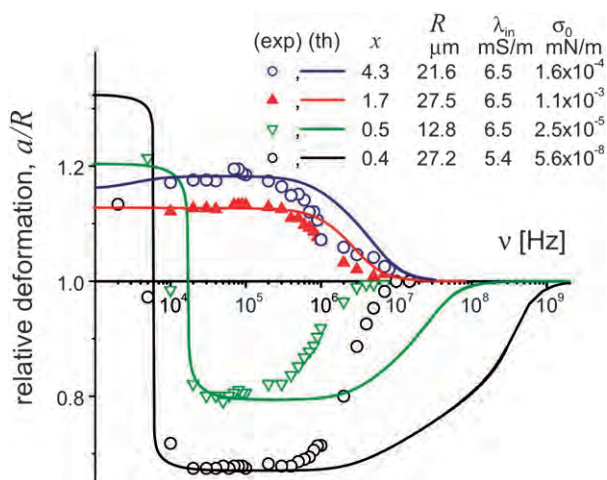

Fig. 3 Comparison between experimental data, symbols (exp), from Aranda *et al.*[48] and theory, solid curves (th), as introduced by eqn (6), for vesicle shapes in AC fields at conditions given in the legend. The initial tension σ_0 is an adjustable parameter for the theoretical curves.
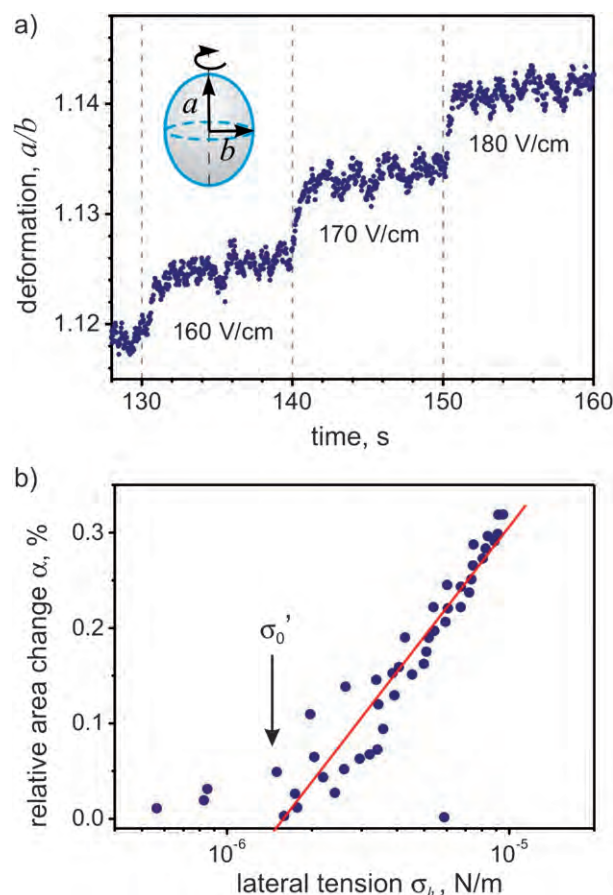

Fig. 4 Vesicle electrodeformation as a method for measuring the membrane bending stiffness. (a) Degree of deformation, a/b (as indicated in the inset) induced on a vesicle made of dipalmitoylphosphatidylcholine : cholesterol 9 : 1 (molar ratio) subjected to AC field with frequency 200 kHz. The applied electrical potential is increased every 10 s with a step of 0.5 V (10 V/cm), as indicated. The first two seconds after changing the field are excluded from averaging over the shape in time. (b) Relative area change of a vesicle subjected to AC field (300 kHz) as a function of the membrane tension. Each data point is a result of averaging the relative area change over 90 images. The solid line is a linear least squares fit, which slope yields $\kappa = (9.5 \pm 0.6) \times 10^{-20}$ J for the bending stiffness and the intercept gives $\sigma_0' = (1.7 \pm 1.4) \times 10^{-6}$ N/m.

the following 3–8 s can be time-averaged to achieve better precision in a/b. For the conductivity conditions and frequency range (between 1 kHz and 300 kHz) in such experiments, the vesicles adopt prolate deformation as discussed in the previous sections.

The vesicle deformation is associated with a change in the apparent area due to flattening the membrane fluctuations. Area stored in small membrane undulations is pulled out and made optically visible. The changes in apparent area is modulated by the membrane tension[50,51] (note that this equation is equivalent to eqn (7)):

$$\alpha \equiv \frac{A - A_0}{A_0} = \frac{k_B T}{8\pi\kappa} log\left(\frac{\sigma_h}{\sigma_0'}\right) \qquad (8)$$

where A is the area of the ellipsoid, A_0 is the area of the sphere with the same volume, and σ_0' is the positive parameter obtained by extrapolation to $\alpha = 0$. Note that σ_0' can be larger than the

actual tension at zero field strength. The tension of the deformed vesicle, σ_h, can be obtained from the electric stresses. The normal electric stress at the equator of the vesicle as given in the work of Helfrich and coworkers[28,30] is:

$$(T_{rr})_{eq} = -\frac{9}{8}\varepsilon_w E_0^2 \qquad (9)$$

where ε_w is the dielectric constant of water, and E_0 is the field strength far away from the vesicle. Since the pressure inside the vesicle must be constant, combining the Laplace equation at the poles and in the equator gives

$$(c_1 + c_2)_{eq}\sigma_h - (T_{rr})_{eq} = (c_1 + c_2)_{pole}\sigma_h \qquad (10)$$

where c_1, c_2 are the principal curvatures taken either at the equator (eq) or the pole (pole), and therefore measurable from the geometry of the vesicle.

Logarithmic plot of the membrane lateral tension obtained from eqn (10) against the change in apparent area gives a straight line with slope related to the bending rigidity as described in eqn (8). One example of this protocol applied to a vesicle composed of dipalmitoylphosphatidylcholine and cholesterol is given in Fig. 4b. A linear least squares fit of the dependence of the relative area change as a function of the applied tension following eqn (8) yields for the slope $\kappa = 9.5 \times 10^{-20}$ J. Repeating the measurement on the same vesicle shows reproducibility within about 22% deviation from the value of κ. Scatter within about 25% is observed when the measurements are performed on different vesicles with the same composition. The obtained value for the bending stiffness is consistent with published data.[52]

Note that this method does not apply to vesicles containing charged lipids and for vesicles embedded in salt solutions. In these cases, the Maxwell stress tensor used to evaluate the membrane tension has to account for the media conductivity (as discussed in the previous two sections) and the charges at the membrane surface.

3.2 Electrohydrodynamic flows in vesicles induced by non-homogeneous AC fields

As discussed above, electric fields induce forces at the vesicle interface, due to the difference in the media polarizabilities. At intermediate frequencies, $1/t_c < \omega < \omega_{MW}$, as shown in section 3.1, the lateral force is responsible for the vesicle deformation. In addition, this force may also lead to fluid flows, analogous to the flows induced in liquid droplets.[53] However, there is a fundamental difference between droplets and vesicles, which arises from the properties of the lipid bilayer.[54] The membrane behaves as a two dimensional nearly incompressible fluid. Under stress, it develops tension to keep its surface area constant. In uniform AC fields, membrane flow in the vesicle is not expected because the lateral electric stress is counterbalanced by the resulting axially symmetric gradient in the membrane tension. In inhomogeneous fields however, this force balance is broken and a flow of lipids occurs in order to restore it. Note that in most experimental conditions used for electromanipulation, vesicles, cells or other particles are exposed to inhomogeneous fields, arising from screening by neighboring particles, sedimentation or chamber geometry.

To study the lipid flow dynamics in AC fields, we used giant vesicles with mixed lipid bilayers, which, at room temperature, phase separate in liquid ordered (l_o) and liquid disordered (l_d) phases,[55] leading to the formation of l_o and l_d domains on the vesicles. A small fraction of fluorescent dye was added, which preferentially partitions in the l_d phase. The lipid ratio was such that the l_o phase appeared as dark circular patches in the surrounding fluorescently labeled l_d phase.

The membrane flow pattern was resolved by following the motion of the l_o patches with confocal microscopy.[56] The top or the bottom part of the vesicle were recorded as shown on the micrographs in Fig. 5a–c. The inner and outer vesicle solutions were 0.1 M sucrose and glucose, respectively. This ensures osmotic balance, i.e. constant vesicle volume, and causes the vesicles to sediment at the bottom of the chamber. The electric field was applied between two parallel cylindrical electrodes with a diameter of 200 μm and an inter-electrode gap of 500 μm. In AC fields, smaller vesicles experience lifting due to negative dielectrophoretic forces, but the larger ones ($R \geq 50$ μm), also being heavier, remain at the chamber bottom. The proximity of the bottom glass to the vesicle, as shown in Fig. 5d, leads to an asymmetric field distribution at the membrane surface. The field strength is much higher at the lower vesicle part, facing the glass, than at the top part.[56]

Such asymmetric field distribution leads to special membrane flow patterns, consisting of concentric closed trajectories organized in four symmetric quadrants, each extending from the bottom to the top of the vesicle; see Fig. 5d, e. The flow is fastest
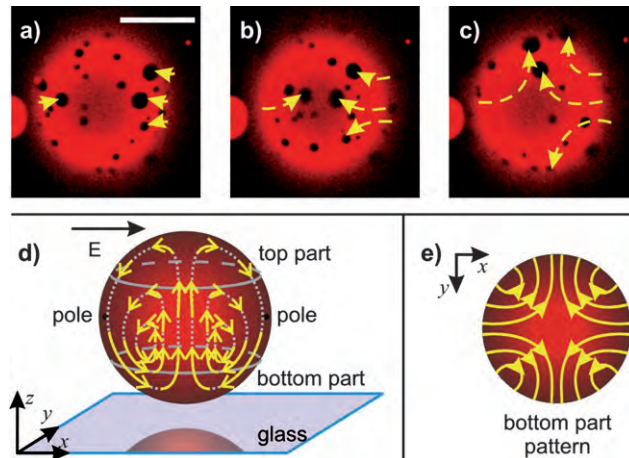

Fig. 5 Micrographs obtained on a confocal microscope (fully opened pinhole) illustrating the membrane flow on the bottom part (a–c) of a giant vesicle with a diameter of about 150 μm induced by an AC field (360 V/cm, 80 KHz), at external and internal conductivities of 25 mS/m and 0.3 mS/m, respectively. The vesicle was prepared from a mixture of dioleoylphosphatidylcholine : dipalmitoylphosphatidylcholine : cholesterol, 4.8 : 3.2 : 2 in mole fractions. The time between the consecutive snapshots is approximately 1.3 s. The yellow dashed arrows indicate the trajectories of selected domains in the consecutive snapshots. The scale bar corresponds to 50 μm. The vesicle is located close to the bottom of the observation chamber as illustrated in (d), where the vesicle top and bottom parts, the poles and the field direction are indicated. The side and the bottom views of the flow lines are sketched in (d) and (e), respectively. The length of the arrows in (d) roughly corresponds to the amplitude of the flow velocity.
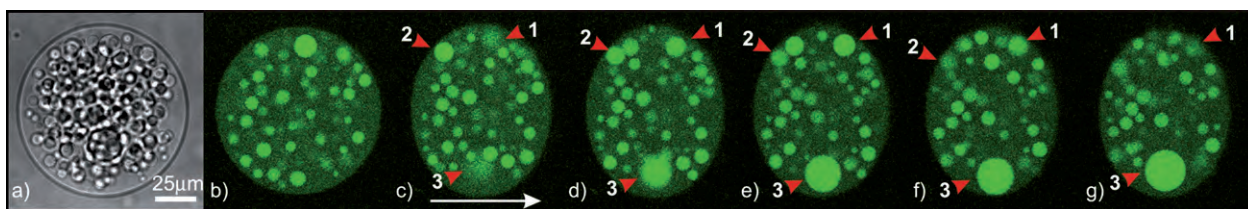
Fig. 6 (a) A phase-contrast image and (b–g) confocal cross sections of a giant lipid vesicle enclosing dextran-rich droplets (green fluorescence) in a PEG-rich phase. The cross section in (b), corresponding to the image in (a), is taken close to the equatorial plane of the vesicle and shows only the droplets in focus. Application of an inhomogeneous AC field (460 V/cm, 80 KHz) at an external conductivity of 40 mS/m leads to a vesicle shape deformation and an internal flow in the direction perpendicular to the plane of the image (c–g). The flow is visualized by following the motion of droplets 1, 2 and 3, which come in focus and go out of focus. The time period is 2.5 s between images (c–d) and (d–e) and 5 s between (e–f) and (f–g). The field direction is indicated by the arrow in (c).

at the periphery of the quadrant and at the bottom of the vesicle. The top and the bottom of the vesicle are stagnation points. The velocity of the domains reaches about 30 μm/s corresponding to laminar flows. The velocity can be further increased by the field strength and the conductivity of the external solution. Interesting effects are observed when the field frequency is varied. At frequencies less than about 3 MHz, the motion in the circular trajectories is directed downwards past the poles and upwards along the equator as sketched in Fig. 5d but reverses its direction at higher frequencies.[56]

Calculations of the lateral electric stress or surface force density on the membrane suggest that the vesicle experiences significant shear stress in the vicinity of the solid substrate.[56] As a result, a non-uniform and non-symmetric membrane tension builds up. It triggers lipid flow towards the regions of highest tension, in analogy to Marangoni flows in monolayers.

The flow in the membrane is coupled to fluid flows in the internal and external media. To visualize the effect of the membrane flow on the internal medium we used vesicles containing aqueous solution of the water-soluble polymers poly-(ethylene glycol) (PEG) and dextran. At specific polymer concentration, this solution undergoes phase separation[57,58] producing droplets of dextran-rich phase, which can be visualized *e.g.* by fluorescently labeled dextran. The droplets gradually coarsen. Before the coarsening is completed we subject such vesicles to non-uniform AC fields. As expected, the droplets move since they are coupled to the membrane flow. Therefore, when a cross section of the vesicle is observed with confocal microscopy as in Fig. 6, the droplets are observed to come into focus and to go out of focus again.

Membrane labelling *via* domains allows visualization of lipid motion and this approach should be helpful in order to elucidate other membrane phenomena such as membrane dynamics during electroformation of vesicles, or in the membrane behavior in vesicles subjected to shear flows[59] or mechanical stresses. Furthermore, the AC field-induced flows in the membrane and the interior of the vesicles may find application in microfluidic technologies. We have already demonstrated the effectiveness of the membrane flow for lipid mixing.[56]

4. Vesicle response to DC pulses

As discussed in section 3, vesicles exposed to AC fields can adopt stationary shapes. The application of DC pulses induces short-lived shape deformations. We have previously explored the characteristic times associated with vesicle relaxation and poration,[60,61] as well as electrofusion of vesicles induced by DC pulses.[62,63] This section will be dedicated to some novel observations in this direction. In particular, we will discuss the influence of several other factors on the vesicle response to DC pulses: (i) presence of charged lipids in the membrane, see section 4.1; (ii) particles in the vesicle solution, see section 4.2; and (iii) phase state of the membrane, see section 4.3. Finally, we will introduce an interesting new application of electrofusion, namely for the synthesis of nanoparticles in vesicles; see section 4.4.

4.1 Unusual behavior of charged membranes exposed to DC pulses: vesicle bursting

Strong electric pulses applied to single component giant vesicles made of phosphatidylcholine induce the formation of pores, which reseal within milliseconds.[60] The mechanism of this pore formation, *i.e.*, electroporation, can be understood in terms of the stress in the bilayer created by the electric field.[32] In the presence of this field, the accumulated charges across the membrane create a transmembrane potential, which induces an effective electrical tension[19,60,64] as defined by the Maxwell stress tensor. Fluid membranes rupture if the tensions exceed about 10 mN/m[19,65] also known as lysis tension.

Studying phosphatidylcholine membranes is motivated by the fact that phosphatidylcholines are the most abundant lipids found in mammalian cells. In order to better mimic biological membranes, we investigated the behavior of multi-component vesicles containing a fraction of negatively charged lipids in different medium conditions.[66]

Two different types of charged vesicles were used: vesicles composed of mixtures of synthetic or natural lipids. In the first case, palmitoyloleoylphosphatidylcholine (POPC) and palmitoyloleoylphosphatidylglycerol (POPG), which is negatively charged, were used. In the second case, the vesicles were made of lipid extract (LE) from the plasma membrane of red blood cells, which contains approximately 10 mol% anionic lipids, mainly phosphatidylserines. When working with charged membranes, the medium pH and ionic strength are very important, as they can tune the bilayer electrostatic properties. Thus, three types of solutions for the vesicle preparation were considered: water, 1 mM Hepes buffer (pH 7.4) with 0.1 mM EDTA, and 0.5 mM NaCl, which provides the same ionic strength as the buffered

solution. Below, we refer to these solutions as non-buffered, buffered and salt solutions, respectively. To ensure good optical contrast, the vesicles in all preparations also contained 0.2 M sucrose inside and isotonic glucose solution outside.

Under certain conditions, POPC : POPG mixtures behave in the same way as pure PC vesicles,[60] *i.e.*, the pulses induce opening of macropores with a diameter up to about 10 μm, which reseal within 50 ms. This behavior was observed for mixed vesicles in buffered solutions at all molar ratios used: 9 : 1, 4 : 1 and 1 : 1, and for non-buffered or salt solutions at low POPG content (9 : 1 and 4 : 1). A very surprising response was observed for 1 : 1, POPC : POPG vesicles in non-buffered and salt solutions: they disintegrated after electroporation;[66] see Fig. 7a. Typically, one macropore formed and expanded in the first 50–100 ms at a very high speed of approximately 1 mm/s. The entire vesicle content is released and is seen as darker liquid in Fig. 7a. In order to better resolve the membrane reorganization after rupture, we used fluorescent labeling and confocal microscopy, as shown in Fig. 7b. The bursting was followed by restructuring of the membrane into what seemed to be interconnected bilayer fragments in the first seconds, and a tether-like structure in the first minute. Then the membrane stabilized into interconnected micron-sized tubules and small vesicles. These observations suggest that the vesicle bursting and membrane instability is related to the large amount of POPG in the bilayer and to the medium. No vesicle disintegration was observed in buffered solution and for lower content of POPG. Thus, we considered the hypothesis that vesicle bursting and membrane instability is related to the charged state of the bilayer.[67–69]

Interestingly, LE vesicles behave in the same way as synthetic 1 : 1, POPC : POPG vesicles. Conventional poration–resealing was observed in buffered solution, whereas the unusual bursting occurred in non-buffered and salt solutions. These results suggest that the bursting is not specific to PG but to the charged state of the membrane. The LE membranes contained approximately 10 mol% anionic lipids, which was enough to induce membrane destabilization. In the synthetic membranes 50 mol% of PG was needed to lead to the same effect.

The amount of PG in the bilayer is not the only factor triggering bursting of the synthetic membranes. In particular, vesicles with the same high content of PG (50 mol%) do not burst in buffered solution. Even though the main difference between buffered solution and the non-buffered and salt solutions seems to be the pH, significant protonation of PG should occur only for pH lower than 5.5, which is below the working pH values in this study. Thus, with respect to pH, the solutions are not very different.

As already mentioned, the ionic strengths of the buffered and the salt solutions were identical. Then, strictly speaking, the only composition difference between the two solutions is the presence of Hepes (1 mM) and EDTA (0.1 mM) in the buffer. To test which of the two components was responsible for preventing the bursting, we prepared giant vesicles (GUVs) composed of 1 : 1, POPC : POPG in 1 mM Hepes only as well as in 0.1 mM EDTA only. The experiments show that vesicles burst in the presence of 1 mM Hepes (without EDTA). On the other hand, in solutions containing 0.1 mM EDTA the conventional poration–resealing behavior was observed. Thus, EDTA is the essential component preventing vesicle bursting induced by the electric pulse. EDTA is a chelating agent, which is generally added in solutions to bind possible multivalent ions present as impurities in the solution, like calcium.[70] However, supplementing the 0.1 mM EDTA vesicle solution with excess of $CaCl_2$ (0.5 mM) to block the EDTA did not recover the bursting phenomenon.

Plasma membranes should exhibit similar bursting behavior as that of the LE vesicles, because their lipid composition is similar. However, cell membranes are subjected to internal mechanical constraints imposed by the cytoskeleton, which prevents their disintegration even if their membranes are prone to disruption when subjected to pulses. Instead, the pores in the cell membrane are stable for a long time[71] and can either lead to cell death by lysis or reseal depending on the media.[8,72] The latter is the key to efficient electroporation-based protocols for drug or gene transfer in cells. The results reported here suggest that membrane charge as well as minute amounts of molecules such as EDTA might be important but not yet well understood regulating agents in these protocols.

4.2 Vesicle behavior in the presence of nanoparticles

Gold and silver nanoparticles, as well as quantum dots are attractive tools for visualizing processes in cells. One possible application involves their employment in optical trapping as handles for force measurements inside living cells.[73,74] Another appealing feature is that magnetic and charged particles can be manipulated by electromagnetic fields. Thus, we were interested in the response of lipid membranes to electric fields in the presence of nanoparticles. For this purpose, we used GUVs made from the conventional lipid egg lecithin (L-α-phosphatidylcholine), and gold nanoparticles, 80 nm in diameter. The vesicles were electroformed in a sucrose solution and subsequently diluted in an isotonic glucose solution containing the particles at a concentration up to 2.2×10^{10} particles/ml. We applied DC pulses with a duration of 200 μs and a field strength of 3.4 kV/cm.
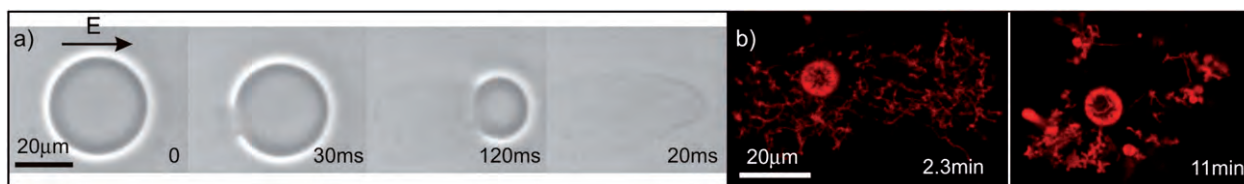

Fig. 7 Bursting of charged (POPC : POPG, 1 : 1) vesicles subjected to electric pulses. The time after the beginning of the pulse is marked on each image. (a) Phase contrast microscopy snapshots from fast camera observation of a vesicle in salt solution subjected to a pulse with field strength 1.2 kV/cm and duration 200 μs. The field direction is indicated in the first snapshot. The vesicle bursts and disintegrates. (b) Confocal cross-sections of a vesicle, which has been subjected to an electric pulse and has burst and rearranged into a network of tubes and smaller vesicles.
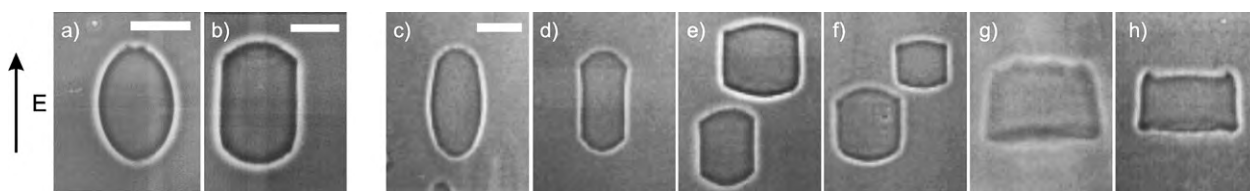
Fig. 8 Vesicle response to DC pulses in the presence and absence of salt and gold particles. The direction of the field is indicated by the arrow on the left. The first snapshot (a) shows a vesicle deformation in the absence of salt and particles. In this case, the DC pulse duration is 200 μs and the field strength is 1.4 kV/cm. The applied pulse is sufficient to porate the vesicle as visualized by dark eruptions of sucrose solution leaking out of the vesicle. In the presence of 0.03 mM salt in the vesicle exterior and no particles present, the vesicles adopt cylindrical shapes as shown in (b). In the latter, the DC pulse duration is 200 μs and the field strength is of 2 kV/cm. Snapshots (c) to (h) show vesicles deforming in the presence of 80 nm gold particles for a DC pulse with a duration of 200 μs and a field strength of 3.4 kV/cm. The gold concentration was successively increased from 1.1×10^8 particles/ml in (c), to 5.5×10^8 in (d), 1.1×10^9 in (e), 2.2×10^9 in (f), 1.1×10^{10} in (g), and 2.2×10^{10} particles/ml in (h). There is a clear concentration dependence of the shape adopted by the deformed vesicles. Snapshots (a), (c), (e) and (f) were taken 150 μs after the beginning of the pulse and (b), (d), (g) and (h) after 200 μs. All scale bars correspond to 15 micrometres.

Previous work, where GUVs were exposed to DC pulses, has shown cylindrical deformations when salt was present in the vesicle exterior;[61] note that in the absence of salt in the external solution, the vesicles deform only into prolates, see Fig. 8a. By applying a DC pulse and systematically varying the concentration of gold nanoparticles outside the vesicles, we observed very similar morphologies. Since the lifetime of these cylindrical deformations is very short, between a few hundred microseconds and a few milliseconds, we used a fast digital camera recording at 20 000 frames per second, *i.e.*, an acquisition speed that corresponds to one image every 50 μs.

By varying the concentration of gold nanoparticles in the surrounding media, we could influence the shape adopted by a vesicle exposed to a DC pulse, as shown in Fig. 8c–h. We observed an overall elongation or contraction of the GUV in the direction of the electric field. The images in Fig. 8c–h show how the vesicles respond to an increase in the concentration of gold nanoparticles. It should be noted that the particles are only present in the external medium. For the lowest explored concentration $c_{min} = 1.1 \times 10^8$ particles/ml, shown in Fig. 8c, the vesicles exhibit a similar behavior as in the absence of ions or particles, compare with the image in Fig. 8a. The vesicles elongate only in the direction of the field into a prolate shape. By increasing the gold concentration we could observe a flattening of the vesicle equatorial region; the vesicles adopt the shape of a cylinder with rounded caps. This is similar to the vesicle response in the presence of ions; compare with the image in Fig. 8b. The particle concentration influences the type of the cylindrical deformations observed. At concentrations slightly above c_{min}, the vesicles adopt tube-like shapes parallel to the direction of the electric field. When the gold concentration was increased tenfold, $10 \times c_{min}$, coexistence of "discs" and "tubes" occurred during the DC pulse, some of them almost looking "square" (Fig. 8e, f). At even higher particle concentrations, the vesicles adopted only a disc-like shape (Fig. 8g, h).

Parallels can be drawn between the above observations and the prolate and oblate shapes of vesicles subjected to AC fields described in section 3.1, but even more so to the shapes adopted by vesicles subjected to DC pulses in the presence of NaCl.[61] The overall behavior is the same, disc-like, square-like or tube-like deformation depending on the outer (and inner) salt or particle

concentration conditions. This suggests that the deformation mechanism in the presence of gold nanoparticles and salt is the same. Indeed, both ions and particles are charged. By measuring the electrophoretic mobility of the gold colloids, we could estimate their zeta potential to be slightly below −50 mV. This would indicate that the nanoparticles migrate towards the anode during the DC pulse. In the case of salt, Na^+ and Cl^- move in opposite directions, while the gold colloids move only in one direction. This might explain the observed asymmetry in the deformed vesicles, especially at the higher particle concentrations where the vesicles adopt a disc-like shape with a trapezoidal cross section; see Fig. 8g and h. The area of the side of the disc facing the anode seems to be larger than the one facing the cathode.

As discussed in a previous report,[61] one possible explanation could be that ions or particles flatten the equatorial zone of the deformed vesicle. At least during the first part of the pulse there is an inhomogeneity in the membrane tension due to the fact that the electric field is the strongest at the poles of the vesicle, and almost zero close to the equator. The kinetic energy of the accelerated ions hitting the equatorial region of the vesicle is higher than the energy needed to bend the membrane, thus leading to the observed deformation. In addition, particle-driven flows may be inducing membrane instability giving rise to higher order modes of the vesicle shape.[75] Yet another possible explanation may be related to a change in the spontaneous curvature of the bilayer due to the particle (or ion) asymmetry across the membrane.[76] During the pulse, local and transient accumulation of particles in the membrane vicinity can occur. The mechanism driving the cylindrical deformations might be a combination of nanoparticle electrophoresis and changes in the membrane spontaneous curvature.

The idea that the balance between the particle concentration in the inner and outer media influences the type of deformation is supported by the observation that repeated exposure of the same vesicles to many consecutive DC pulses leads to coexistence between "tubes" and "discs". Poration of the lipid membrane is frequent at these pulse strengths and durations[60] and depends, among other factors, on the vesicle radius and proximity to the electrode, *e.g.* larger vesicles porate at weaker pulses than smaller ones. The pulses might induce permeation of gold particles into the interior of some of the vesicles, which would explain the variation in the cylindrical deformations.

In summary, when subjected to DC pulses, vesicles in the presence of nanoparticles respond similarly to vesicles in salt solutions.[61] The mechanisms behind these responses are still to be clarified, and it remains to be seen whether the processes governing them are the same.

4.3 Electrodeformation and poration of vesicles in the gel-phase

In the previous two sections, the response of membranes in the fluid state has been discussed. The mechanical and rheological properties of such membranes differ significantly from those of membranes in the gel-phase; for a concise comparison see Dimova et al.[77] For example, the bending stiffness and the shear surface viscosity of gel-phase membranes are orders of magnitude higher than those of membranes in the fluid phase,[78–81] and membranes in the gel-phase are thicker.[82] These differences introduce new features in the response of gel-phase membranes to electric fields, which we discuss next.

We studied POPC and dipalmitoylphosphatidylcholine (DPPC) membranes, which undergo their main transition at −2 °C and 41.6 °C, respectively. We compared the response to square wave DC pulses of a POPC vesicle, which at room temperature is in the fluid phase, with the response of a vesicle made of DPPC, which is in the gel-phase. The applied DC pulses were weak enough not to induce formation of microscopic pores in the membranes and no leakage of the internal sucrose solution outside the vesicle was observed. Fig. 9 shows the deformation of one POPC and one DPPC vesicle in response to DC pulses 300 µs long. The deformation is characterized by the ratio of the two semiaxes, a/b, of the vesicles. To achieve similar maximal degree of deformation, stronger pulses had to be applied to the gel-phase vesicle as compared to the fluid one. Pulses with field strength about 1 kV/cm produce deformations in gel-phase vesicles, which are not detectable optically, while strong pulses about 5 kV/cm applied to the fluid-phase vesicles cause poration. The latter influences the relaxation dynamics.[60] Note that the

degree of deformation depends on the initial vesicle tension and excess area,[60] which are both unknown a priori.

The responses of the two vesicles differ significantly. The fluid vesicle gradually deforms and reaches maximum deformation at the end of the pulse. The gel-phase vesicle responds significantly faster, and exhibits a relaxation with a decay time of about 30 µs during the pulse. To our knowledge, such intra-pulse relaxation has not been previously reported. The vesicles had similar size and were both in salt-free solutions with conductivity of about 1 mS/m. For a fluid vesicle with radius $R = 20$ µm, the charging time is $t_c \cong 550$ µs, see eqn (2), i.e., longer than the pulse duration. Gel-phase membranes are thicker, and thus, have lower membrane capacitance,[83] leading to charging times shorter or comparable to the duration of the pulse. The faster response of the gel-phase vesicle as shown in Fig. 9 correlates with the shorter charging time as compared to the fluid vesicle.

After the end of the pulse, the relaxation of the gel DPPC vesicle is also much faster than that of the fluid membrane. The relaxation behavior depends on whether the membrane was porated or not.[60] In the example given in Fig. 9, no microscopic pores were detected, but it is plausible that in the gel-phase vesicle pores with sizes in the sub-optical range were formed during the pulse. The formation of such pores may explain the intra-pulse relaxation in the vesicle deformation.

If DC pulses of field strength larger than the discussed above are applied, the gel-phase vesicles rupture: the pores resemble micrometre-sized cracks on a solid shell.[32] Contrary to pores in fluid membranes, which reseal within tens of milliseconds,[60] the cracks in gel-phase vesicles are stable and seem not to reseal.

Understanding the response of the gel-phase membranes will require thorough consideration of the membrane mechanical and rheological properties as well as the interaction of electric fields with such membranes. Both the intra- and after-pulse relaxations of the vesicles in gel-phase are poorly understood and will be the object of further investigation.

4.4 Vesicle electrofusion as a method for nanoparticle synthesis in vesicles

Strong electric pulses induce electrical breakdown of fluid lipid bilayers leading to formation of transient pores. The vesicles become permeable for a certain time. When two such porated vesicles are in close contact, fusion can occur. The concept to fuse two GUVs in order to initiate content mixing reactions has been proposed earlier.[84,85] In this section, we introduce the application of fusion of giant vesicles for the synthesis of nanoparticles in closed compartments.

The principle of fusion-mediated synthesis is simple: the starting reagents are separately loaded into different vesicles, and then the reaction is triggered by the fusion of these vesicles, which allows the mixing of their contents. The success of this approach is guaranteed by two important factors. First, the lipid membrane is impermeable to the reactants such as ions or macromolecules. Second, fusion can be initiated by a variety of fusogens such as membrane stress,[86,87] ions or synthetic fusogenic molecules,[62,88–90] fusion proteins,[91] laser beam radiation,[85] or electric fields.[63,92] Among the fusion methods listed above, electrofusion becomes increasingly important because of its reliable, fast and easy handling.[63] An immediate benefit of this strategy is
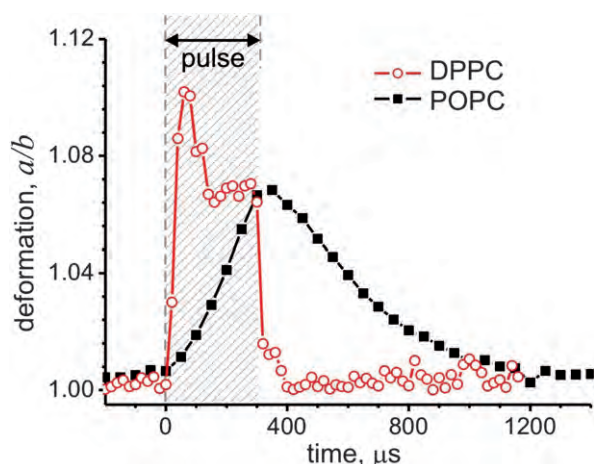

Fig. 9 Deformation response of a gel-phase DPPC vesicle with a radius of 22 µm, and a fluid phase POPC vesicle with a radius of 20 µm to DC pulses with a duration of 300 µs. The pulse duration is indicated by the shaded zone. The field strength of the pulses was 5 kV/cm and 0.8 kV/cm for the DPPC and the POPC vesicle, respectively.
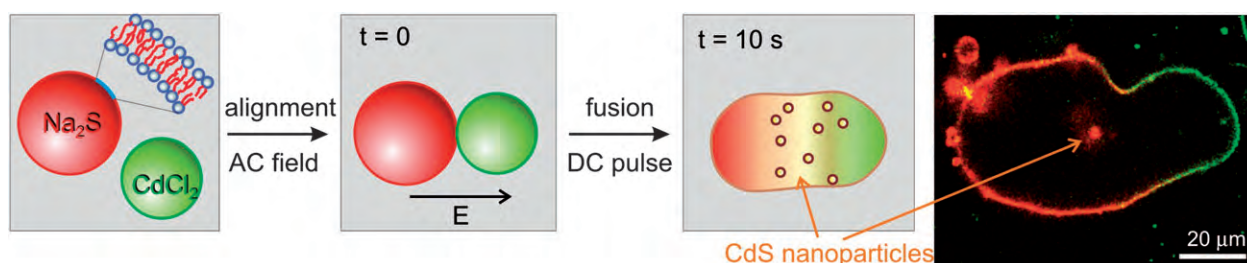
Fig. 10 Electrofusion of vesicles as a method for nanoparticle synthesis: vesicles containing Na_2S and fluorescently labelled in red, and vesicles containing $CdCl_2$, labelled in green, are mixed in Na_2S- and $CdCl_2$-free environment and subjected to an AC field to align them in the direction of the field and bring them close together. A DC pulse initiates the electrofusion of the two vesicles and the reaction between Na_2S and $CdCl_2$ proceeds to the formation of CdS nanoparticles encapsulated in the fused vesicle. The last snapshot is a confocal scan of a vesicle obtained by fusion of a vesicle loaded with 0.3 mM Na_2S (red part of the fused vesicle) and a vesicle loaded with 0.3 mM $CdCl_2$ (labelled in green). The fluorescence signal from the synthesized CdS nanoparticles in the vesicle interior is visible as indicated by the arrow.[94]

that the precise temporal and spatial control on the synthesis process can be easily achieved.

According to our electrofusion protocol, two vesicle populations are mixed, one loaded with Na_2S and labeled with one fluorescent dye (red), the other loaded with $CdCl_2$ and labeled differently (green). The vesicle external media is Na_2S- or $CdCl_2$-free, which can be achieved either by significant dilution of the starting vesicle solutions or by exposure to ion-exchange resins. Application of AC field aligns the vesicles in the direction of the field due to dielectric screening, similarly to pearl-chain formation in suspensions of cells.[15] In order to monitor the nanoparticle formation process, we locate a red-and-green vesicle couple (approximately half of the couples fall in this category) and apply a DC pulse strong and long enough to porate each of the vesicles. For egg lecithin vesicles, pulses of 0.5–2 kV/cm field strength and 150–300 μs duration are sufficient. The steps of this protocol are schematically illustrated in Fig. 10.

Fluorescence in the interior of the fused vesicle was observed, see Fig. 10, which indicates formation of CdS nanoparticles. Fluorescence in the wavelength range between 400 and 800 nm has been previously reported for CdS particles with diameters in the range 1–25 nm.[93] Because the confocal sections show only fluorescence from a thin slice of the vesicle, out of focus fluorescence, which might be emitted from the upper and lower part of the vesicle, is not detected. The obtained product was also investigated using transmission electron microscopy and selected area electron diffraction, which showed the presence of dispersed nanoparticles of diameters ranging between 4 and 8 nm.[94] A noticeable advance of the above approach is that the whole reaction could be viewed and monitored in real time under the optical microscope.

Cells and microorganisms are able to synthesize inorganic nanoparticles.[95–97] The tentative interpretation of this observation is related to the involvement of specific molecules such as inorganic-binding peptides.[98–100] Our experiments suggest that nanoparticles could be synthesized in biological compartments even without the mediation of biomacromolecules. For example, the fusion of small vesicles with the cell membranes could be a possible mechanism for the cell-based synthesis of nanoparticles. The necessary condition according to such a scenario is that the vesicles are loaded with one reagent, while the local concentration of the other chemical at the cell is suitably matched. Low concentrations in the submillimolar range are sufficient to produce CdS nanoparticles.[94]

In general, vesicle fusion provides many unexplored opportunities for protein biosynthesis, enzyme-catalyzed reactions, and biomineralization processes.[101]

5. Conclusions

The results reported in this review demonstrate that cell-sized giant vesicles provide a very useful model for resolving the effect of electric fields on lipid membranes because vesicle dynamics can be directly observed with optical microscopy. We have examined the behavior of giant vesicles exposed to AC fields of various frequencies and elucidated the underlying physical mechanism for the vesicle deformations as well as stress-induced lipid flows in inhomogeneous AC fields. We have shown that the vesicle response to electric fields can be exploited to evaluate the mechanical properties of the membrane.

Until recently, the dynamics of vesicle relaxation and poration, which occur on microsecond time-scales, has eluded direct observation because the temporal resolution of optical microscopy observations with analog video technology is in the range of milliseconds. We used fast digital imaging to discover new features in the membrane response arising from the presence of charged lipids in the membrane, nanoparticles in the surrounding media, and compared the response of gel-phase membranes to fluid ones. Finally, we introduced a novel application of membrane electrofusion, which allowed us to perform nanoparticle synthesis in vesicles.

In conclusion, the reported observations demonstrate that giant vesicles can help advance fundamental knowledge about the complex behavior of cells and membranes in electric fields and can inspire novel practical applications.

References

1 *Electromanipulation of cells*, ed. U. Zimmermann and G. A. Neil, CRC Press, Boca Raton, 1996.

2 *Electroporation and electrofusion in cell biology*, ed. E. Neumann, A. E. Sowers and C. A. Jordan, Plenum Press, New York, 1989.

3 *Guide to electroporation and electrofusion*, ed. D. C. Chang, B. M. Chassey, J. A. Saunders and A. E. Sowers, Academic Press, New York 1992.

4 R. H. W. Funk and T. K. Monsees, *Cells Tissues Organs*, 2006, **182**, 59–78.

5 J. Voldman, *Annu. Rev. Biomed. Eng.*, 2006, **8**, 425–454.

6 M. Zhao, B. Song, J. Pu, T. Wada, B. Reid, G. P. Tai, F. Wang, A. H. Guo, P. Walczysko, Y. Gu, T. Sasaki, A. Suzuki, J. V. Forrester, H. R. Bourne, P. N. Devreotes, C. D. McCaig and J. M. Penninger, *Nature*, 2006, **442**, 457–460.

7 J. Teissie, M. Golzio and M. P. Rols, *Biochim. Biophys. Acta*, 2005, **1724**, 270–280.

8 E. Tekle, R. D. Astumian and P. B. Chock, *Proc. Natl. Acad. Sci. U. S. A.*, 1994, **91**, 11512–11516.

9 R. Heller, R. Gilbert and M. J. Jaroszeski, *Adv. Drug Deliv. Rev.*, 1999, **35**, 119–129.

10 A. Gothelf, L. M. Mir and J. Gehl, *Cancer Treat. Rev.*, 2003, **29**, 371–387.

11 R. Nuccitelli, U. Pliquett, X. Chen, W. Ford, R. J. Swanson, S. J. Beebe, J. F. Kolb and K. H. Schoenbach, *Biochem. Biophys. Res. Commun.*, 2006, **343**, 351–360.

12 L. M. Mir, P. Devauchelle, F. Quintin-Colonna, F. Delisle, S. Doliger, D. Fradelizi, J. Belehradek Jr and S. Orlowski, *Brit. J. Cancer*, 1997, **76**, 1617–1622.

13 M. Golzio, J. Teissié and M. P. Rols, *Proc. Natl. Acad. Sci. U. S. A.*, 2002, **99**, 1292–1297.

14 M. Golzio, M. P. Rols and J. Teissié, *Methods*, 2004, **33**, 126–135.

15 U. Zimmermann, *Rev. Physiol. Biochem. Pharmacol.*, 1986, **105**, 176–256.

16 J. Teissie and T. Y. Tsong, *Biochemistry*, 1981, **20**, 1548–1554.

17 R. W. Glaser, S. L. Leikin, L. V. Chernomordik, V. F. Pastushenko and A. I. Sokirko, *Biochim. Biophys. Acta*, 1988, **940**, 275–287.

18 S. Kakorin, T. Liese and E. Neumann, *J. Phys. Chem. B.*, 2003, **107**, 10243–10251.

19 D. Needham and R. M. Hochmuth, *Biophys. J.*, 1989, **55**, 1001–1009.

20 D. V. Zhelev and D. Needham, *Biochim. Biophys. Acta*, 1993, **1147**, 89–104.

21 O. Sandre, L. Moreaux and F. Brochard-Wyart, *Proc. Natl. Acad. Sci. U. S. A.*, 1999, **96**, 10591–10596.

22 E. Tekle, R. D. Astumian, W. A. Friauf and P. B. Chock, *Biophys. J.*, 2001, **81**, 960–968.

23 C.-H. Lee, Y.-F. Chang, C.-H. Tsai and P.-H. Wang, *Langmuir*, 2005, **21**, 7186–7190.

24 M. Winterhalter and W. Helfrich, *J. Colloid Interface Sci.*, 1988, **122**, 583–586.

25 P. Peterlin, S. Svetina and B. Žekś, *J. Phys.: Condens. Matter.*, 2007, **19**, 136220.

26 H. Engelhardt, H. Gaub and E. Sackman, *Nature*, 1984, **307**, 378–380.

27 M. Mitov, P. Méléard, M. Winterhalter, M. I. Angelova and P. Bothorel, *Phys. Rev. E.*, 1993, **48**, 628–631.

28 M. Kummrow and W. Helfrich, *Phys. Rev. A*, 1991, **44**, 8356–8360.

29 W. Harbich and W. Helfrich, *Z. Naturforsch. A*, 1979, **34**, 1063–1065.

30 G. Niggemann, M. Kummrow and W. Helfrich, *J. Phys. II*, 1995, **5**, 413–425.

31 S. Lecuyer, W. Ristenpart, O. Vincent and H. Stone, *Appl. Phys. Lett.*, 2008, **92**, 104105.

32 R. Dimova, K. A. Riske, S. Aranda, N. Bezlyepkina, R. L. Knorr and R. Lipowsky, *Soft Matter*, 2007, **3**, 817–827.

33 T. B. Jones, *Electromechanics of particles*, Cambridge University Press, New York, 1995.

34 H. P. Schwan, in *Interaction between EM fields and cells*, ed. A. Chiabrera, C. Nivolin and H. P. Schwan, Plenum Press, 1985, pp. 75–97.

35 C. Grosse and H. P. Schwan, *Biophys. J.*, 1992, **63**, 1632–1642.

36 H. Engelhardt and E. Sackman, *Biophys. J.*, 1988, **54**, 495–508.

37 A. W. Friend Jr., E. D. Finch and H. P. Schwan, *Science*, 1975, **187**, 357–359.

38 F. J. Iglesias, M. C. Lopes, C. Santamaria and A. Dominguez, *Biophys. J.*, 1985, **48**, 712–726.

39 M. I. Angelova and D. S. Dimitrov, *Faraday Discuss. Chem. Soc.*, 1986, **81**, 303–311.

40 M. I. Angelova, S. Soleau, P. Meleard, J.-F. Faucon and P. Bothorel, *Prog. Colloid Polym. Sci.*, 1992, **89**, 127–131.

41 D. J. Estes and M. Mayer, *Biochim. Biophys. Acta*, 2005, **1712**, 152–160.

42 T. Pott, H. Bouvrais and P. Meleard, *Chem. Phys. Lipids*, 2008, **154**, 115–119.

43 L. R. Montes, A. Alonso, F. M. Goni and L. A. Bagatolli, *Biophys. J.*, 2007, **93**, 3548–3554.

44 P. Taylor, C. Xu, P. D. I. Fletcher and V. N. Paunov, *Phys. Chem. Chem. Phys.*, 2003, 1732–1733.

45 P. Taylor, C. Xu, P. D. I. Fletcher and V. N. Paunov, *Chem. Commun.*, 2003, **5**, 4918–4922.

46 M. I. Angelova, in *Giant Vesicles*, ed. P. L. Luisi and P. Walde, John Wiley & Sons Ltd., Chichester, 2000, ch. 3, pp. 27–43.

47 P. Sens and H. Isambert, *Phys. Rev. Lett.*, 2002, **88**, 128102.

48 S. Aranda, K. A. Riske, R. Lipowsky and R. Dimova, *Biophys. J.*, 2008, **95**, L19–L21.

49 P. M. Vlahovska, R. S. Gracià, S. Aranda and R. Dimova, *Biophys. J.*, 2009, **96**, 4789–4803.

50 W. Helfrich and R. M. Servuss, *Nuovo Cimento D*, 1984, **3**, 137–151.

51 E. Evans and W. Rawicz, *Phys. Rev. Lett.*, 1990, **64**, 2094–2097.

52 J. J. Pan, T. T. Mills, S. Tristram-Nagle and J. F. Nagle, *Phys. Rev. Lett.*, 2008, **100**, 198103.

53 G. I. Taylor, *Proc. R. Soc. London, Ser. A*, 1966, **291**, 159–166.

54 D. Lacoste, G. I. Menon, M. Z. Bazant and J. F. Joanny, *Eur. Phys. J. E*, 2009, **28**, 243–264.

55 S. Veatch and S. Keller, *Phys. Rev. Lett.*, 2002, **89**, 268101.

56 M. Staykova, R. Lipowsky and R. Dimova, *Soft Matter*, 2008, **4**, 2168–2171.

57 M. Helfrich, L. K. Mangeney-Slavin, M. S. Long, K. Djoko and C. D. Keating, *J. Am. Chem. Soc.*, 2002, **124**, 13374–13375.

58 Y. Li, R. Lipowsky and R. Dimova, *J. Am. Chem. Soc.*, 2008, **130**, 12252–12253.

59 M. Abkarian and A. Viallat, *Soft Matter*, 2008, **4**, 653–657.

60 K. A. Riske and R. Dimova, *Biophys. J.*, 2005, **88**, 1143–1155.

61 K. A. Riske and R. Dimova, *Biophys. J.*, 2006, **91**, 1778–1786.

62 C. K. Haluska, K. A. Riske, V. M. Artzner, J. M. Lehn, R. Lipowsky and R. Dimova, *Proc. Natl. Acad. Sci. U. S. A.*, 2006, **103**, 15841–15846.

63 K. A. Riske, N. Bezlyepkina, R. Lipowsky and R. Dimova, *Biophys. Rev. Lett.*, 2006, **4**, 387–400.

64 I. G. Abidor, V. B. Arakelyan, L. V. Chernomordik, Y. A. Chizmadzhev, V. F. Pastushenko and M. R. Tarasevich, *J. Electroanal. Chem.*, 1979, **104**, 37–52.

65 K. Olbrich, W. Rawicz, D. Needham and E. Evans, *Biophys. J.*, 2000, **79**, 321–327.

66 K. A. Riske, R. L. Knorr and R. Dimova, *Soft Matter*, 2009, **5**, 1983–1986.

67 M. D. Betterton and M. P. Brenner, *Phys. Rev. Lett.*, 1999, **82**, 1598–1601.

68 V. Kumaran, *Phys. Rev. Lett.*, 2000, **85**, 4996–4999.

69 H. Isambert, *Phys. Rev. Lett*, 1998, **80**, 3404–3407.

70 K. A. Riske, H. G. Dobereiner and M. T. Lamy-Freund, *J. Phys. Chem. B*, 2003, **107**, 5391–5392.

71 K. Schwister and B. Deuticke, *Biochim. Biophys. Acta*, 1985, **816**, 332–348.

72 K. Kinosita and T. Y. Tsong, *Nature*, 1977, **268**, 438–441.

73 P. M. Hansen, V. K. Bhatia, N. Harrit and L. Oddershede, *Nano Lett.*, 2005, **5**, 1937–1942.

74 L. Jauffred, A. C. Richardson and L. B. Oddershede, *Nano Lett.*, 2008, **8**, 3376–3380.

75 V. Kantsler, E. Segre and V. Steinberg, *Phys. Rev. Lett.*, 2007, **99**, 178102.

76 R. Lipowsky and H.-G. Dobereiner, *Europhys. Lett.*, 1998, **43**, 219–225.

77 R. Dimova, S. Aranda, N. Bezlyepkina, V. Nikolov, K. A. Riske and R. Lipowsky, *J. Phys.: Condens. Matter*, 2006, **18**, S1151–S1176.

78 T. Heimburg, *Biochim. Biophys. Acta*, 1998, **1415**, 147–162.

79 R. Dimova, B. Pouligny and C. Dietrich, *Biophys. J.*, 2000, **79**, 340–356.
80 C.-H. Lee, W.-C. Lin and J. Wang, *Phys. Rev. E*, 2001, **64**, 020901.
81 K. R. Mecke, T. Charitat and F. Graner, *Langmuir*, 2003, **19**, 2080–2087.
82 J. F. Nagle and S. Tristram-Nagle, *Biophys. Biochem. Acta*, 2000, **1469**, 159–195.
83 M. A. Stuchly, S. S. Stuchly, R. P. Liburdy and D. A. Rousseau, *Phys. Med. Biol.*, 1988, **33**, 1309–1324.
84 D. T. Chiu, C. F. Wilson, F. Ryttsen, A. Stromberg, C. Farre, A. Karlsson, S. Nordholm, A. Gaggar, B. P. Modi, A. Moscho, R. A. Garza-Lopez, O. Orwar and R. N. Zare, *Science*, 1999, **283**, 1892–1895.
85 S. Kulin, R. Kishore, K. Helmerson and L. Locascio, *Langmuir*, 2003, **19**, 8206–8210.
86 F. S. Cohen, M. H. Akabas and A. Finkelstein, *Science*, 1982, **217**, 458–460.
87 J. C. Shillcock and R. Lipowsky, *Nat. Mater.*, 2005, **4**, 225–228.
88 D. J. Estes, S. R. Lopez, A. O. Fuller and M. Mayer, *Biophys. J.*, 2006, **91**, 233–243.
89 B. R. Lentz, *Eur. Biophys. J.*, 2007, **36**, 315–326.
90 M. Kunishima, M. Tokaji, K. Matsuoka, J. Nishida, M. Kanamori, K. Hioki and S. Tani, *J. Am. Chem. Soc.*, 2006, **128**, 14452–14453.
91 R. Jahn, T. Lang and T. C. Südhof, *Cell*, 2003, **112**, 519–533.
92 A. Strömberg, F. Ryttsén, D. T. Chiu, M. Davidson, P. S. Eriksson, C. F. Wilson, O. Orwar and R. N. Zare, *Proc. Natl. Acad. Sci. U. S. A.*, 2000, **97**, 7–11.
93 H. Weller, *Angew. Chem.*, 1993, **105**, 43–55.
94 P. Yang, R. Lipowsky and R. Dimova, *Small*, DOI: 10.1002/smll.200900560.
95 D. Bhattacharya and R. K. Gupta, *Crit. Rev. Biotechnol.*, 2005, **25**, 199–204.
96 C. Sanchez, H. Arribart, M. Madeleine and G. Guille, *Nat. Mater.*, 2005, **4**, 277–288.
97 D. Mandal, M. E. Bolander, D. Mukhopadhyay, G. Sarkar and P. Mukherjee, *Appl. Microbiol. Biotechnol.*, 2006, **69**, 485–492.
98 N. Kröger, M. B. Dickerson, G. Ahmad, Y. Cai, M. S. Haluska, K. H. Sandhage, N. Poulsen and V. C. Sheppard, *Angew. Chem.*, 2006, **118**, 7397–7401.
99 N. Kröger, M. B. Dickerson, G. Ahmad, Y. Cai, M. S. Haluska, K. H. Sandhage, N. Poulsen and V. C. Sheppard, *Angew. Chem., Int. Ed.*, 2006, **45**, 7239–7243.
100 R. R. Naik, S. J. Stringer, G. Agarwal, S. E. Jones and M. O. Stone, *Nat. Mater.*, 2002, **1**, 169–172.
101 P. Walde and S. Ichikawa, *Biomol. Eng.*, 2001, **18**, 143–177.